



Effects of hydrolysis degree on the formation of ferroelectric-core fillers and the electric performance of polyvinyl alcohol composites

Yunyun Yang^{a,b,c,1}, Lei Huang^{b,1}, Yusen Zhao^c, Zijin Yan^b, Ximin He^{c,*}, Xufu Cai^{b,*}

^a College of Civil Aviation Safety Engineering, Civil Aviation Flight University of China, Civil Aircraft Fire Science and Safety Engineering Key Laboratory of Sichuan Province, Guanghan, 618307, China

^b College of Polymer Science and Engineering, The State Key Laboratory of Polymer Materials Engineering, Sichuan University, Chengdu, 610065, China

^c Department of Materials Science and Engineering, University of California Los Angeles, Los Angeles, CA, 90024, USA

ARTICLE INFO

Keywords:

Ferroelectric-core fillers
Hydrolysis degree
Interfacial interaction
Crystallized phase

ABSTRACT

Dielectric materials have been regarded as an emerging field for dielectric energy storage in the last few decades. To improve the dispersion of high-dielectric-constant fillers in polymer, many methods of surface modification and core-shell structure have been reported focusing on the forming of shell. Here we introduce a soluble ferroelectric [Hdabco]ClO₄ (TEDA.C, dabco = diazabicyclo[2.2.2]octane) into polyvinyl alcohol (PVA) matrix via solution mixing to create a ferroelectric TEDA.C crystal core by the hydrogen bonding between PVA and TEDA.C. We studied the effects of PVA's chain structure on the interfacial interactions between the two components, the crystalline phase of TEDA.C, and the dielectric, ferroelectric, and physical properties of composites by employing three PVAs of different hydrolysis degree. High hydrolysis degree promoted the homogeneous distribution and fine miscibility of TEDA.C in PVA matrix, but also impeded the hydrogen bond movement of TEDA.C, which resulted in the disordered paraelectric phase of ordered-disordered-type ferroelectric. Comparing the dielectric, ferroelectric and physical properties of three PVA systems provides further insights about the hydrolysis degree of PVA benefitting the interfacial interaction and interfacial effects, leading to a potential facile and powerful tool for tuning the properties of PVA composites.

1. Introduction

High-dielectric-constant (high-k) polymer materials have numerous applications in organic field-effect transistors (OFETs) [1], organic thin-film electroluminescent devices [2], electrical stress control applications [3], actuators [4], and energy storage devices [5,6]. To improve the dielectric constant of polymer, most of the reported studies have been focused on the addition of inorganic components, including inorganic ferroelectrics [7], metal fillers [8], and carbon nanofiller [9,10]. However, the inorganic fillers tend to aggregate in polymer matrices due to their poor dispersion and compromise the physical performances of polymer materials [11,12]. The surface functionalization of fillers by hydroxylation [13,14], coupling agents [15], surfactants [16], and phosphoric acids [17,18] is used to promote the miscibility and phase stability of polymer composites. However, these additional steps will inevitably cause post-processing issues and potential contamination.

Other options, including in-situ polymerization [19–21] and introducing core-shell structure fillers [22–24] to raise the dispersion of filler in composite, are more complex and difficult to be applied on a large scale.

Perovskite-type ferroelectrics [25,26] are commonly used to increase the dielectric constant of polymer due to their spontaneous polarization and ample dipoles. Compared to inorganic ferroelectrics, ferroelectrics with organic molecular components [27] as another kind of ferroelectrics, have spontaneous polarization and dipoles, have broader curie temperature tunability and essential characteristic for the design of all-organic electronics [28–31]. In the work of Bayer and colleagues [27] fabricated six all-organic high-k solution processable composites by incorporating an organic ferroelectric crystal, thiourea, suggesting the enhancements of ferroelectric crystal for dielectric properties. In our previous work [30], we also introduced a soluble organic molecular ferroelectrics [Hdabco]ClO₄ (TEDA.C, dabco = diazabicyclo[2.2.2]octane) to modify PVA for enhanced dielectric properties. The hydrogen

* Corresponding author.

** Corresponding author.

E-mail addresses: ximinhe@ucla.edu (X. He), caixf2008@scu.edu.cn (X. Cai).

¹ Yunyun Yang and Lei Huang contributed equally to the work.

Table 1

Compositions of the PVA composite thin films, the value of 1750, 1788 and 1799 are the degree of polymerization and the hydrolysis degree (17 refers to the degree of polymerization of 1700, 50, 88 and 99 refer to the percentage of hydrolysis degree).

Sample	Percentage of Weight				The ratio of TEDA.C:PVA
	1750PVA	1788PVA	1799PVA	TEDA.C	
1750PVA	100	–	–	0	0:100
5T@1750PVA	95.3	–	–	4.7	5:100
10T@1750PVA	90.9	–	–	9.1	10:100
15T@1750PVA	87	–	–	13	15:100
20T@1750PVA	83.3	–	–	16.7	20:100
1788PVA	–	100	–	0	0:100
5T@1788PVA	–	95.3	–	4.7	5:100
10T@1788PVA	–	90.9	–	9.1	10:100
15T@1788PVA	–	87	–	13	15:100
20T@1788PVA	–	83.3	–	16.7	20:100
1799PVA	–	–	100	0	0:100
5T@1799PVA	–	–	95.3	4.7	5:100
10T@1799PVA	–	–	90.9	9.1	10:100
15T@1799PVA	–	–	87	13	15:100
20T@1799PVA	–	–	83.3	16.7	20:100

bonding between PVA and TEDA.C helps TEDA.C form uniformly-dispersed, needle-like core in PVA matrix. Addition of 9.1 wt % ferroelectric TEDA.C increases the dielectric constant of 1788PVA composites by 10 times at 10^7 Hz.

However, the core formation in polymer composites is important yet under-investigated. In this work, we emphasized the effects of hydrolysis degree of PVA on the TEDA.C distribution, crystal morphology and phase. Interestingly, it is found that the abundant hydroxy groups change the cooperative alignment of permanent dipole moments [32, 33] of hydrogen-bonded TEDA.C. In addition, the increasing hydrolysis degree results in phase transition of TEDA.C crystal from ferroelectric phase to paraelectric phase. Meanwhile, the dielectric properties, the ferroelectric properties, and the physical properties of PVA composites are systematically investigated in three PVA systems with different hydrolysis degrees, showing the significant modification effects of hydrolysis degree on the TEDA.C.

2. Experimental

2.1. Materials

1,4-Diazabicyclo[2.2.2]octane hexahydrate (TEDA, $C_6H_{12}N_3 \cdot 6H_2O$ AR), distilled water and perchloric acid ($HClO_4$ GR) were supplied by Kelong Chemical Reagent Corp (Chengdu, China). Polyvinyl alcohol 1750PVA (Mn = 1700, and hydrolysis degree = 50%), 1788PVA (Mn = 1700, and hydrolysis degree = 88%) and 1799PVA (Mn = 1700, and hydrolysis degree = 99%) were supported by Shanghai Titan Scientific Co. Ltd. All reagents and solvents in the syntheses were of reagent grade and used without further purification.

2.2. Samples preparation

The biaxial molecular ferroelectric TEDA.C was prepared by slow evaporation of the ethanol solution of 1,4-diazabicyclo[2.2.2]octane hexahydrate and $HClO_4$ in a 1:1 M ratio [34]. The powder of TEDA.C was dissolved in distilled water to form a solution with a solubility of 240 mg/ml. The PVA powder with different hydrolysis degree was dissolved in distilled water to form a solution with a solubility of 60 mg/ml. The above four solutions were then mixed at a series of different ratios (0 wt% – 16.7 wt% TEDA.C) under magnetic stirring for 60 min (100 rpm) and sonication for 30 min to prepare precursor solution. Subsequently, the mixed solution was added dropwise to a treated glass

substrate and dried in a 50 °C vacuum oven for 24 h. During the evaporation of water, the TEDA.C crystals were formed in situ in the PVA matrix. The thin films were then transferred to a mold, followed by the hot press at a temperature of 373 K and pressure of 10 MPa for 8 min, and eventually cooled to room temperature with maintaining pressure at 5 MPa. In this work, the content of films was listed in Table 1.

2.3. Instrumentation

Optical microscope photographs of PVA films were obtained by using polarized light microscope (BX51, Olympus corporation). The films for characterizations had a thickness of $0.08 \text{ mm} \pm 0.005 \text{ mm}$. X-ray diffraction (XRD, Ultima IV) was carried out using Cu K α radiation with 40 KV/40 mA. The dielectric property was carried out with a broad frequency dielectric spectrometer Concept 50 (NOVOCONTROL, Germany). The diameter and thickness of the film samples were $12.5 \pm 0.1 \text{ mm}$ and $0.08\text{--}0.10 \text{ mm}$, respectively. Polarization-electric field (P-E) hysteresis loops were measured on Radiant Ferroelectric Tester (Premier) for different voltage cycles at 10 Hz, 100 Hz and 1000 Hz, respectively. Breakdown strength of PVA samples was measured at room temperature by applying AC voltage ramp with a rate of increase of 200V/s. The Ultraviolet-Visible Near-Infrared spectrum was recorded using a UV-3600 (Shimadzu, Japan) spectrometer at room temperature with a scanning wavelength ranging from 200 to 800 nm. The mechanical properties were measured on an Instron 5567 machine with a 10 kN load cell at a 20 mm/min loading rate. The measurement of TGA was carried out using a Netzsch TG209 F1 thermogravimeter at a linear heating rate of 10 K/min. Samples (about $8.0 \pm 0.2 \text{ mg}$) were heated in the temperature range from 300 K to 800 K, with a controlled dry nitrogen flow of 60 ml/min.

3. Results and discussion

The polarized optical microscopy (POM) images of a series of PVA films and PVA with TEDA.C composite films (referred to as composite films in this work) are shown in Fig. 1. The POM images of the pure PVA films with different hydrolysis degrees are uniform, indicating that PVA has dominant amorphous phase. By embedding TEDA.C in 1750PVA, the TEDA.C crystal is not obviously anisotropic at low TEDA.C concentration but significantly accumulates with increasing TEDA.C concentration. Instead, TEDA.C in 1788PVA forms rod-like crystals at low TEDA.C addition. Increasing TEDA.C concentration increases the length and diameter of crystals, and dendritic structure crystals is generated when the TEDA.C concentration is above 9.1 wt% (which is the same as the crystalline structure of TEDA.C in Fig. S2). For 1799PVA, TEDA.C crystallizes as a lamellar structure stacked layer by layer. These results show the considerable effects of the hydrolysis degree on the crystal morphology and distribution of TEDA.C in PVA. The distribution of TEDA.C has also been confirmed by the FTIR-ATR technique. The observed strong FTIR-ATR peaks of TEDA.C in 20 T@1750PVA curve (Fig. S3, Fig. S4) suggest the poor distribution of TEDA.C in 1750PVA, which is corresponding to TEDA.C aggregating on the 1750PVA surface. Other similar FTIR-ATR curves in Fig. S5 and Fig. S6 imply the good covering ability of 1788PVA and 1799PVA.

We then studied the material crystalline structure by X-ray diffraction (XRD). Regarding the pure TEDA.C film, the XRD peaks' position and pattern remain unchanged at a temperature below 393 K, above which the ferroelectric phase transits to the paraelectric phase (Fig. S7). This phase transition of TEDA.C is reversible, indicated by the presence of the ferroelectric phase pattern again when cooling the temperature from 413 K to 373 K. The reversible phase transition can also be verified by Differential Scanning Calorimeter (DSC) (Fig. S8). After confirming the phase transition and structure of pure TEDA.C, we have conducted XRD for PVA and composite films (Fig. 2). The XRD pattern of neat 1750PVA, 1788PVA, and 1799PVA have a similar peak around 20° , indicating the semicrystalline structure of PVA. For the composite films,

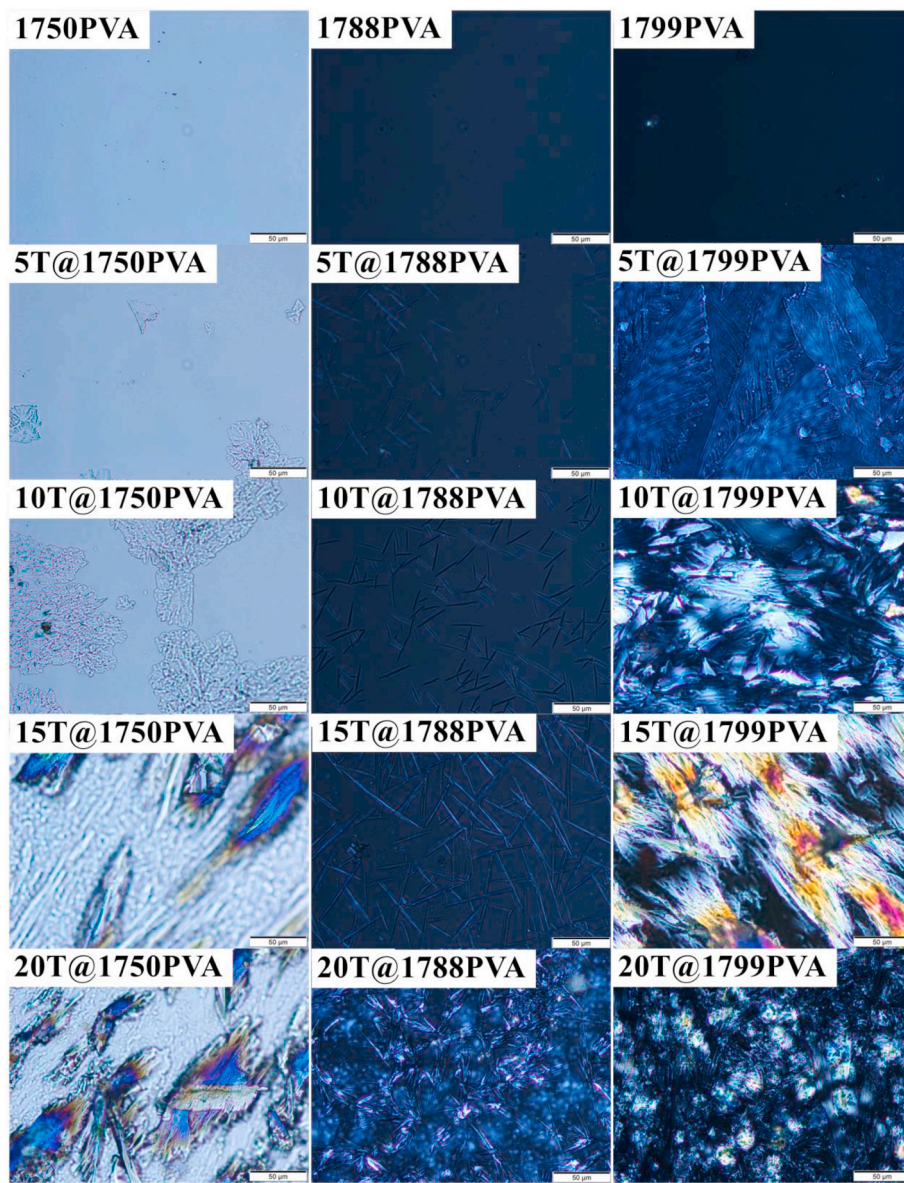


Fig. 1. The POM images of PVA films.

the TEDA.C peak intensity increases with the TEDA.C addition. Interestingly, TEDA.C peaks' position also shifts in different PVA matrices, indicating the effects of different hydrolysis degree on the crystal structures of TEDA.C. Therefore, we compare the XRD pattern of composite films with 16.7 wt% TEDA.C (corresponding to 20 T@1750PVA) and neat TEDA.C film in Fig. 2a. The XRD peaks of 20 T@1750PVA well agree with the peaks of TEDA.C at 373 K, suggesting the unchanged ferroelectric phase of TEDA.C in 1750PVA. However, the XRD peaks of 20 T@1788PVA are the combination of the TEDA.C pattern at 373 K and 393 K (Fig. S9). Further, the XRD peaks of 20 T@1799PVA are close to the TEDA.C pattern at 393 K (Fig. 2c, Fig. S9). These results indicate that the crystalline phase of TEDA.C is adjusted with the increase of PVA hydrolysis degree isothermally. This phase change is presumably because the PVA with a high hydroxyl-group concentration strongly interacts with TEDA.C by hydrogen bond and impedes the hydrogen bond movement of TEDA.C, which results in the disordered paraelectric phase [35,36] of ordered-disordered-type ferroelectric. These results suggest a new switch of spontaneous electric polarization by tuning the hydrolysis degree of PVA matrix. Notably, the traditional methods to

achieve high phase transition temperature are mainly by molecular modification with new molecular design based on complex ferroelectric compounds [33,36]. Therefore, this facile modification methodology by the hydrolysis degree of PVA matrix is very promising.

We have further studied the dielectric properties of the composite films. The frequency-dependent dielectric constants and dielectric loss of composites films are presented in Fig. 3. With increasing TEDA.C, the peak of dielectric loss shifts to a higher frequency. For 50% hydrolysis degree PVA system, when the TEDA.C addition is up to 13 wt%, the dielectric constants of 15 T@1750PVA shows an exponential growth resulting from more defects for charge accumulation and current pathway. With the increase of hydrolysis degree to 88%, TEDA.C forms evenly dispersed needle-like crystals in 1788PVA. These polar dipoles of ferroelectric-phase crystal benefit the dielectric constant enhancement of 1788PVA (Fig. 3c). In addition to the increased dielectric constant, the dielectric loss also maintains low values with the addition of TEDA.C before 10 Hz as shown in Fig. 3d. With further increasing hydroxyl degree, the hydrogen bonds strongly affect the cooperative alignment of permanent dipole moments [32,33] of TEDA.C and lead to the transition

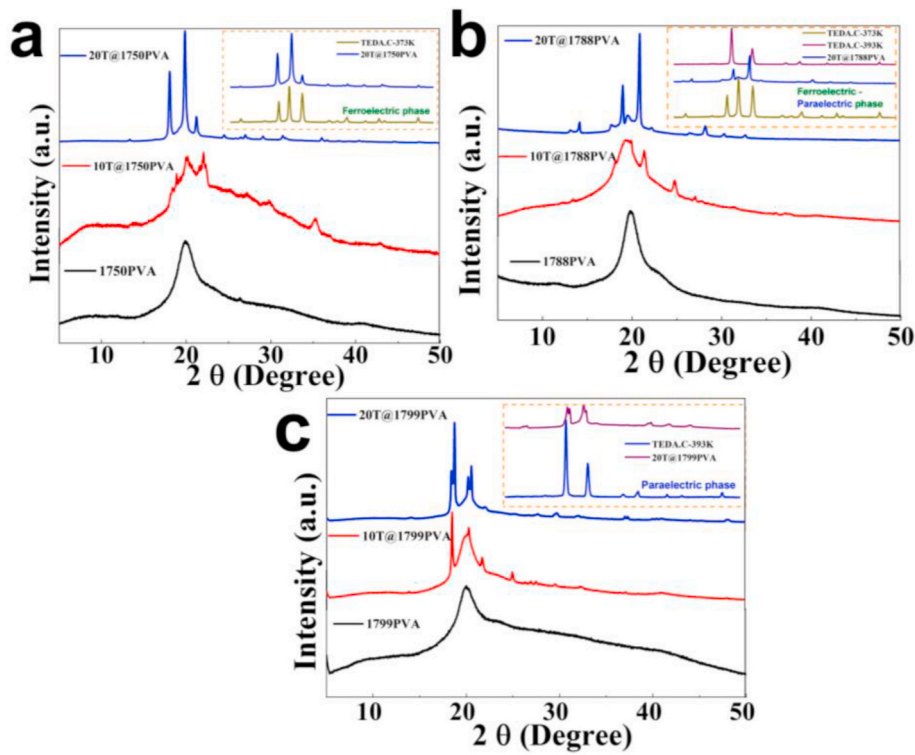


Fig. 2. The XRD images of (a)1750PVA and composite films (b)1788PVA and composite films (c)1799PVA and composite films and their zoom in images TEDA.C patterns(TEDA.C-373 K corresponding to ferroelectric phase, TEDA.C-393 K corresponding to paraelectric phase).

of TEDA.C to paraelectric phase (Fig. 2, Fig. S7). Additionally, strong hydrogen bonding limits the polarization of 1799PVA's hydroxy groups, reducing the dielectric constant of composites. Therefore, the dielectric constants of 1799PVA composites are close to that of pure 1799PVA. Notably, there is an increase in the dielectric constant of 1799PVA composites at low frequency (0.1–100 Hz, Fig. 3e), which can be explained by the Maxwell-Wagner-Sillars (MWS) interfacial polarization [37,38]. Moreover, the high hydrolysis degree helps PVA chains form more micro-crystal which brings the peaks of $\tan\delta$ (Fig. 3d and f).

Fig. 4 shows the imaginary electric modulus (M'') of pure PVA and PVA composites, further distinguishing the effects of hydrolysis degree on dielectric relaxation. The crystalline part α_c -relaxation [39–41] of PVA chains shifts the M'' peaks to high frequency range with increasing measuring temperature. However, in composite films with low hydrolysis degree PVA, the M'' peaks of 10 T@1750PVA shift to lower frequency compared with those of 1750PVA. On the contrary, in composite films with high hydrolysis degree PVA (10 T@1788PVA and 10 T@1799PVA), the M'' peaks shift to a higher frequency (Related value is listed in Table S1). The $1/T$ versus $\ln(f)$ plot are presented in Fig. 4c, f and Fig. 4i, and the parameter value of fitting lines is listed in Table S2. The activation energy (E_a) can be calculated based on equation (1) [42, 43] and the parameter value of fitting lines, as displayed in Fig. 4cfi.

$$f = f_0 \exp(-E_a / (k_B * T)) \quad (1)$$

where E_a is the activation energy, k_B is Boltzmann's constant, T is the absolute temperature, and f is the frequency at the maximum from the imaginary modulus spectrum, respectively.

In low-hydrolysis-degree PVA system, the poor distribution and

accumulation of TEDA.C creates substantial defects, leading to a lower energy (descended by 70%) required for space charge flowing through barriers and aggregates in the composite. By contrast, higher hydrolysis degree PVA possesses more interfacial and charge polarization due to the better core-shell distribution, increasing the activation energy for dielectric relaxation. And the TEDA.C ferroelectric core formed by hydrogen bonds in 1788PVA effectively weakens the gap between 1788PVA and 10 T@1788PVA (reduced by 3%).

Breakdown strength (E_b) is another important electric property for energy storage films. In this part, the breakdown strength of PVA composites under AC electric field with various loading of TEDA.C are shown in Fig. 5, which is evaluated by a two parameter Weibull statistic distribution method [43,44] as below:

$$P(E) = 1 - \exp[-(E/E_0)^\beta] \quad (2)$$

where $P(E)$ is the cumulative probability of electric failure, β is the shape parameter related to the degree of dispersion of the experimental data and a high value of β represents high level of reliability. After calculating, the slope of the fitting line is the shape parameter. According to Table 2, the E_b value of PVA-based ferroelectric composites film declines after the modification by TEDA.C. Here we employ following equation (3) to calculate the maximal energy storage density [45,46] of PVA samples

$$W_{\max} = 0.5 * \epsilon_0 * \epsilon_r * E_b^2, \quad W_{\max} = 1/2 \epsilon_0 \epsilon E^2 \quad (3)$$

where ϵ_0 , ϵ_r and E_b are the vacuum permittivity ($8.85 * 10^{-12} \text{F/m}$), dielectric constant and breakdown strength (breakdown strength under AC electric field are calculated by Weibull statistic distribution in this

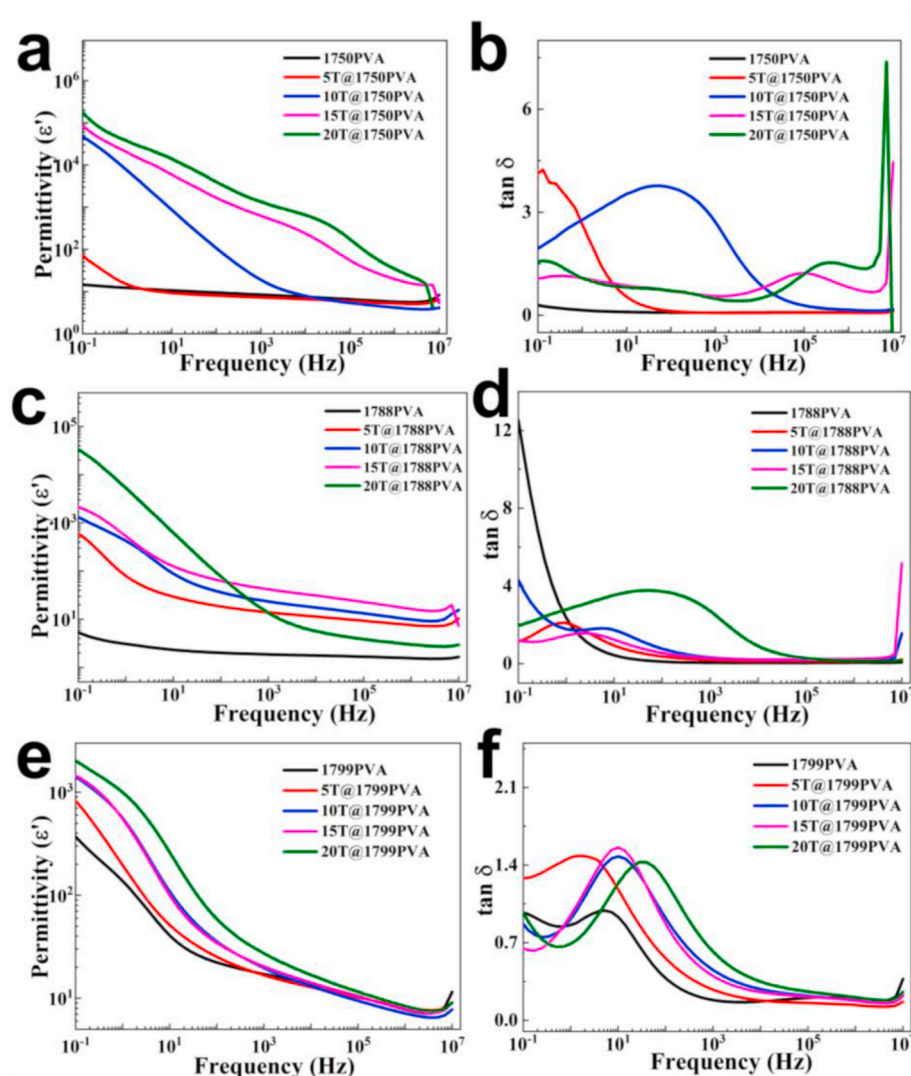


Fig. 3. Frequency dependence of (a, c, e) the real part of complex dielectric constant and (b, d, f) the dielectric loss constant of different hydrolysis PVA films with different content of TEDA.C at 0.1 Hz-10MHz.

work), respectively. And the maximal energy storage density of PVA samples under different frequency are drew in Fig.5bdf. The 15 T@1750PVA and 20 T@1750PVA have the most significant enhancement among three different hydrolysis degree PVA system under low frequency range (0.1–1 kHz), due to the high dielectric constant caused by charge accumulation and current pathway. Except for 5 T@1788PVA, 10 T@1788PVA and 15 T@1788PVA composite films, all other composite films' maximal energy storage density are lower than that of pure PVA films under high frequency range.

The polarization-electric field (P-E) loops of three series of PVA based composites were measured at frequency of 10 Hz, 100 Hz, 1 kHz by ferroelectric workstation and results under the highest electric strength are presented in Fig. S10, respectively. Fig. 6 supply the changes of the residual polarization intensity and coercive electric field of PVA films and PVA composite samples under different frequencies (10, 100, and 1000 Hz) and different electric field. For 50% hydrolysis degree PVA films, the addition of TEDA.C sharply decreases the

polarizing capability of 1750PVA chains. This is because the accumulation of TEDA.C enables charge transport via correlated barrier hopping (according to the dielectric relaxation results) that eliminates charge accumulation in interface and the spontaneous dipoles of ferroelectric TEDA.C's effect. For 88% hydrolysis degree PVA films, polarizing capability is strongly enhanced in 10 T@1788PVA, which is the consequence of the spontaneous dipoles of ferroelectric TEDA.C (Fig. S11). Furthermore, in 99% hydrolysis degree PVA films, the polarization of 1799PVA composites is close to that of pure 1799PVA. The negligible enhancement is because the strong hydrogen bonding between 1799PVA and TEDA.C offsets the polarization effect of 1799PVA and TEDA.C dipoles. Apart from the polarization, we have also compared changes in coercive electric field, which correlated well with the as-mentioned polarization changes (see Fig. 7).

In addition to the dielectric and ferroelectric study, the influence of TEDA.C loading on the transmittance of PVA films are shown in Fig.7-abc. The significant transparency reduction of 1750PVA composites

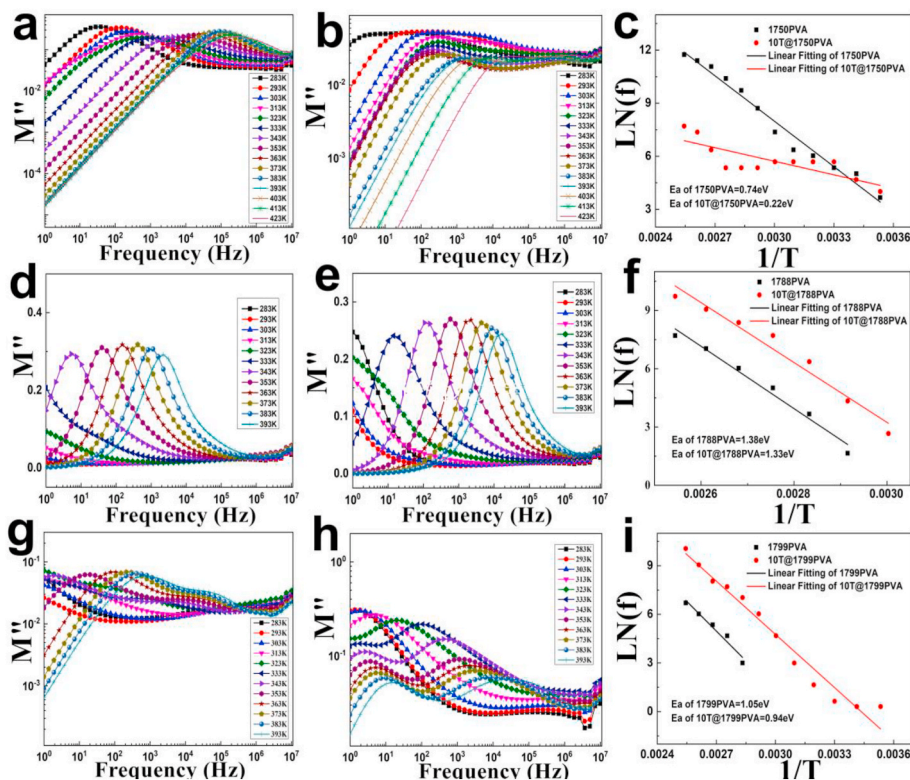


Fig. 4. The frequency dependency of imaginary electric modulus(M'') (a)1750PVA (b)10 T@1750PVA (d)1788PVA (e)10 T@1788PVA (g)1799PVA (h)10 T@1799PVA at different temperature and frequency, and the relationship of $\ln(f_{max})$ versus $1/T$ for (c) 1750PVA and 10 T@1750PVA (f)1788PVA and 10 T@1788PVA (i)1799PVA and 10 T@1799PVA

films is due to the accumulation of TEDA.C on 1750PVA surface. The fine distribution of TEDA.C maintain 1788PVA and 1799PVA composite films 85% and 75% transparency at 4.7 wt% loading. The parameters of the stress-strain curves of films are shown in Fig.7def to illustrate the effects of the distribution of TEDA.C on PVA matrix. With 50% hydrolysis degree, the addition of TEDA.C decreases the tensile stress at breakpoint and the elongation at break, indicating an easier crack formation and propagation during stretching due to the large-scaled phase separation. However, in terms of 1788PVA and 1799PVA composite films, there is a general enhancement in the tensile stress and the stress at the breakpoint with low TEDA.C addition, which is probably caused by the good distribution of TEDA.C. The thermal properties of films were studied by TGA shown in Fig. 8. The addition of TEDA.C in 1750PVA (Figs. 8a) and 1799PVA(Fig. 8e) shifts the initial decomposition stage to a lower temperature, while the decomposition stages of 10 T@1788PVA (Fig. 8c) are consistent with the decomposition stages of 1788PVA. The consistency of the decomposition stage in 88% hydrolysis degree film arises from the well-distributed TEDA.C phase, which maintains the pristine thermal stability and decomposition stages of 1788PVA. The temperature dependency of the $\tan\delta$ and loss modulus by DMA testing for the pure PVA and the TEDA.C-reinforced PVA films are shown in Fig. S12. The enhancements of the loss modulus in 10 T@1788PVA and 10 T@1799PVA are consistent with the enhanced stretchability from stress-strain tests.

4. Conclusions

In summary, we have demonstrated intrinsically stretchable

dielectric composite films by incorporating ferroelectric core, TEDA.C, in PVA matrix with different hydrolysis degrees via solution coating. The effects of chains' structure on composites were systematically studied from the crystalline phase morphologies of TEDA.C and the physical properties of different PVA systems. The PVAs with hydrolysis degree of 88% and 99% facilitated the formation of micrometer-sized rod-like crystal and lamellar grains of TEDA.C uniformly distributing in PVA, whereas film with PVA of 50% hydrolysis degree led to the aggregation of TEDA.C. The crystal morphologies in different PVA matrices were confirmed by XRD, where TEDA.C predominantly formed a ferroelectric phase in low hydrolysis degree PVA and paraelectric phase in high hydrolysis degree PVA. This observation provided a methodology to precisely control the ferroelectric-paraelectric transition of organic molecular ferroelectrics. The results of dielectric constants and dielectric loss at different frequencies and temperatures suggested that a high hydrolysis degree improves the even distribution of TEDA.C, but overly high hydrolysis degree decreases the dielectric constant of the composite film, due to the formation of the paraelectric phase of TEDA.C and hydrogen bonds between TEDA.C and 1799PVA which weakened the polarization of hydroxyl groups. Furthermore, the fine distribution of TEDA.C in 1788PVA and 1799PVA enabled PVA composites to keep good transparency, mechanical properties and thermal stability.

Associated content

Supporting Information includes the characterization of TEDA.C, the temperature dependence of the real part of complex dielectric constant, the imaginary part of complex dielectric constant, the dielectric loss

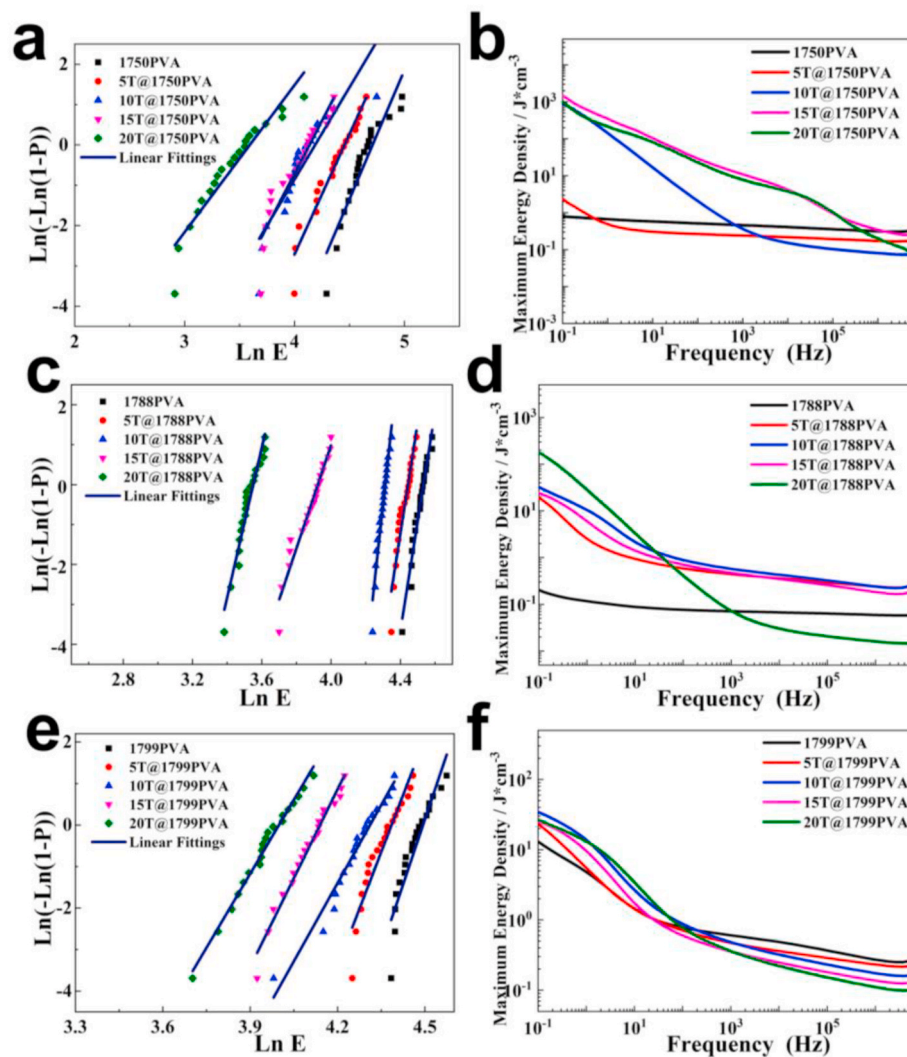


Fig. 5. The Weibull distribution curves of (a)1750PVA composites (c)1788PVA composites (e)1799PVA composites, the dependency of frequency for the calculated maximum energy storage density of (b)1750PVA composites (c)1788PVA composites (f)1799PVA composites with different content of TEDA.C.

Table 2

Weibull parameters and electrical breakdown strength of PVA and PVA composites.

Samples	Intercept	Slope(β)	$\ln E_0$ (-Intercept/Slope)	E_0 (MV/m)
1750PVA	-30.16	6.40	4.71	111.05
5 T @1750PVA	-26.57	5.96	4.46	86.49
10 T @1750PVA	-19.12	4.56	4.19	66.02
15 T @1750PVA	-21.69	5.24	4.14	62.80
20 T @1750PVA	-13.10	3.65	3.59	36.23
1788PVA	-124.11	27.38	4.53	92.76
5 T @1788PVA	-123.15	27.71	4.44	84.77
10 T @1788PVA	-170.74	39.59	4.31	74.44
15 T @1788PVA	-50.70	12.92	3.92	50.40
20 T @1788PVA	-66.73	18.80	3.55	34.81
1799PVA	-93.92	20.90	4.49	89.12
5 T @1799PVA	-80.15	18.28	4.38	79.84
10 T @1799PVA	-54.11	12.55	4.31	74.44
15 T @1799PVA	-59.05	14.26	4.14	62.80
20 T @1799PVA	-47.50	11.88	4.00	54.60

$\tan\delta$, the real part of complex conductivity, the reciprocal of the real part of dielectric modulus and the imaginary part of dielectric modulus of TEDA.C at 1 MHz, 1 KHz and 1 Hz, respectively. The temperature dependency of the $\tan\delta$ and loss modulus by DMA testing for the pure PVA

and the TEDA.C-reinforced PVA films were performed on tensile-molded specimens and were carried out in a dynamic mechanical analyzer (DMA), model Q800 (TA Instruments, USA), equipped with a liquid nitrogen cooling system.

Notes

The authors declare no competing financial interest.

CRedit authorship contribution statement

Yunyun Yang: Data curation, Writing – original draft. **Lei Huang:** Data curation, Writing – original draft. **Yusen Zhao:** Visualization, Investigation. **Zijin Yan:** Data verification and replenishment. **Ximin He:** Conceptualization, Supervision, Writing – review & editing. **Xufu Cai:** Conceptualization, Supervision, Writing – review & editing.

Declaration of competing interest

The authors declare that they have no known competing financial interests or personal relationships that could have appeared to influence the work reported in this paper.

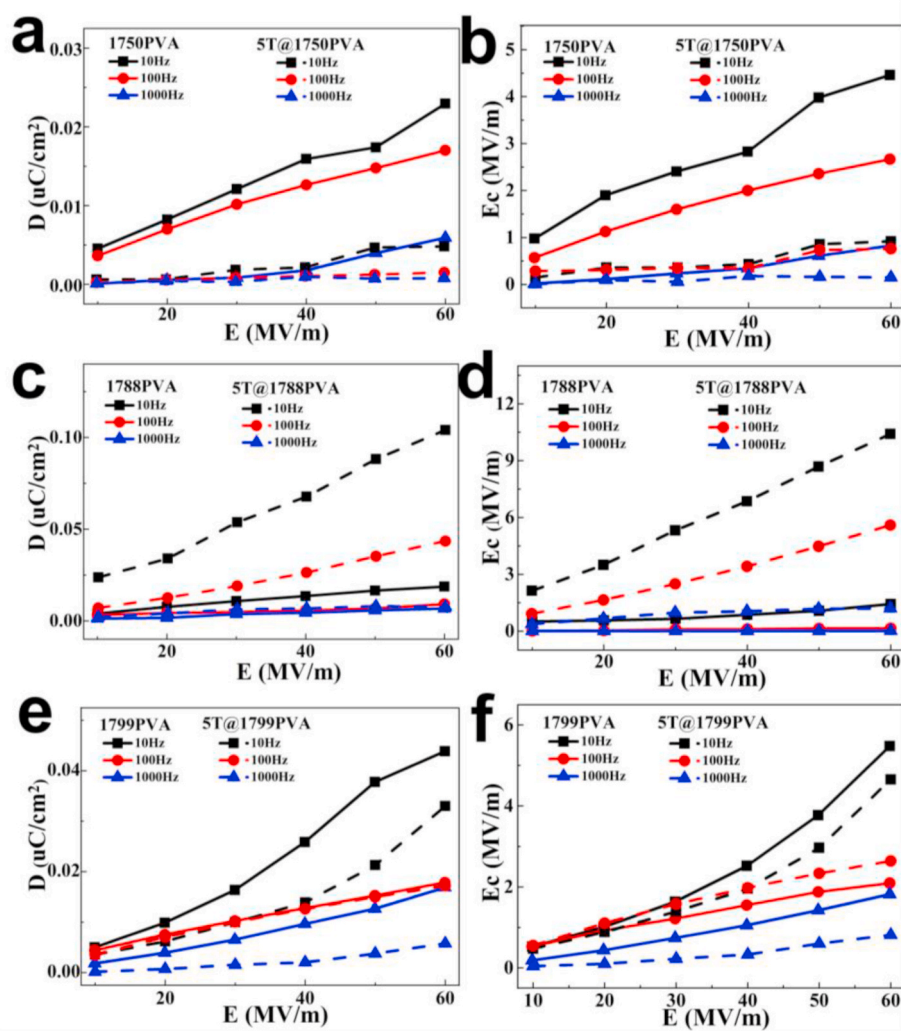


Fig. 6. The trend of residual polarization intensity of (a)1750PVA and 5 T@1750PVA (c)1788PVA and 5 T@1788PVA (e)1799PVA and 5 T@1799PVA, the trend of coercive electric field of (b)1750PVA and 5 T@1750PVA (d)1788PVA and 5 T@1788PVA (f)1799PVA and 5 T@1799PVA under different frequency (10 Hz, 100 Hz, 1000 Hz) and different electric field.

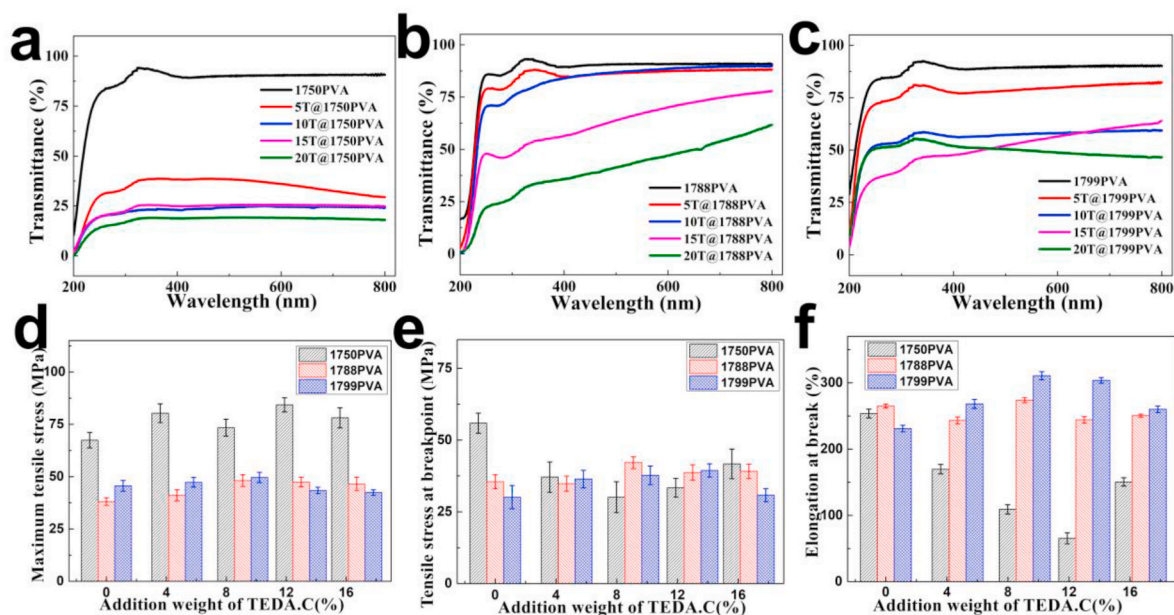


Fig. 7. (a, b, c) Light transmittance curves, (d) The maximum tensile stress, (e) the tensile stress at breakpoint, and (f) the elongation at break of the composite films with different PVA hydrolysis degrees and TEDA.C loadings.

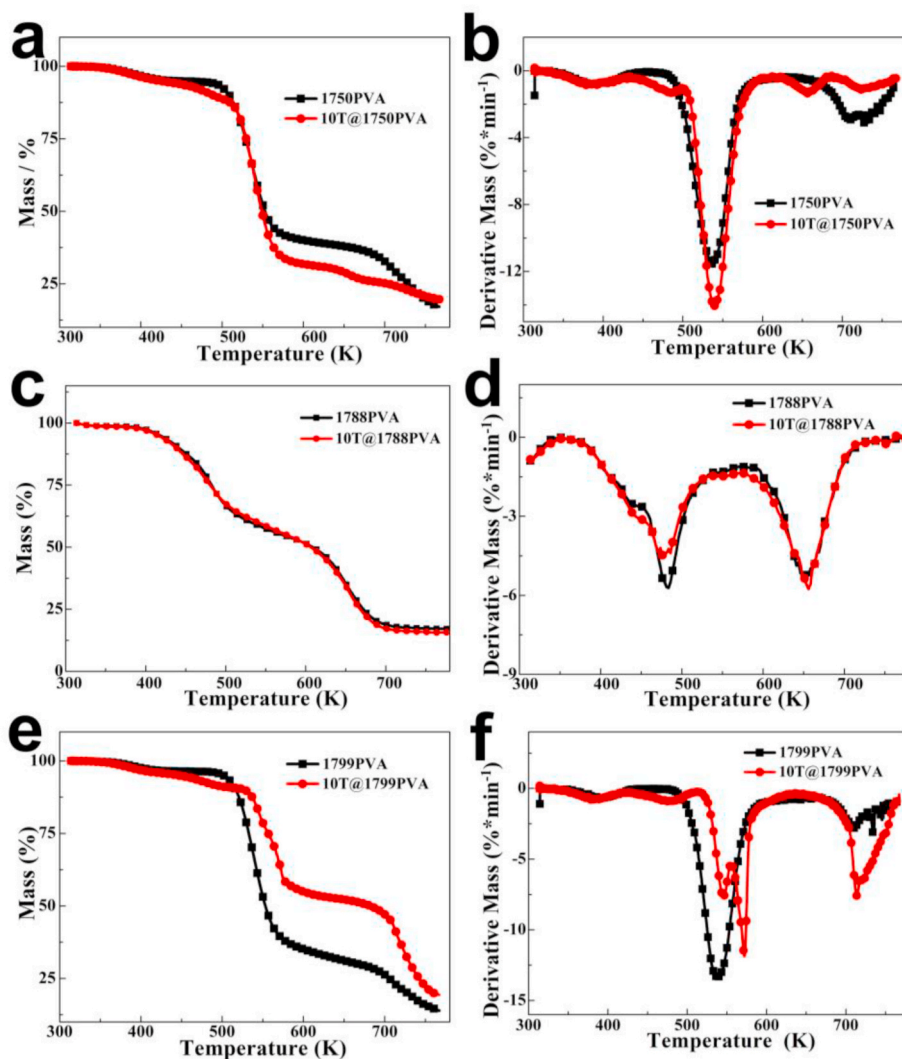


Fig. 8. (a, c, e) The TGA curves of pure PVA and binary PVA composites, (b, d, f) The DTG curves of pure PVA and binary PVA composites under pure nitrogen atmosphere.

Acknowledgments

This work was financially supported by the National Natural Science Foundation of China (NSFC51873114), the Sichuan Science and Technology Program (2021YFSY0001), the National Key R&D Program of China (2018YFC0810600), the Civil Aviation Flight University of China Scientific Research Foundation (J2018-12, J2020-112).

Appendix A. Supplementary data

Supplementary data to this article can be found online at <https://doi.org/10.1016/j.compscitech.2021.109147>.

References

- [1] High and temperature-independent dielectric constant dielectrics from PVDF-based terpolymer and copolymer blends, *Advanced Electronic Materials* 6 (2020), <https://doi.org/10.1002/aem.201901250>.
- [2] Polysiloxane-poly(vinyl alcohol) composite dielectrics for high-efficiency low voltage organic thin film transistors, *J. Mater. Chem. C* 7 (2019) 4879–4886, <https://doi.org/10.1039/c9tc00717b>.
- [3] Role of interface in highly filled epoxy/BaTiO₃ nanocomposites. Part II- effect of nanoparticle surface chemistry on processing, thermal expansion, energy storage and breakdown strength of the nanocomposites, *IEEE Trans. Dielectr. Electr. Insul.* 21 (2014) 480–487, <https://doi.org/10.1109/TDEI.2013.004166>.
- [4] Electrode interface polarization formation in dielectric elastomer actuators, *Sensors and Actuators A Physical* (2020) 312, <https://doi.org/10.1016/j.sna.2020.111992>.
- [5] Facile synthesis of isotactic polyacrylonitrile via template polymerization in interlayer space for dielectric energy storage, *ACS Applied Polymer Materials* 2 (2020) 775–781, <https://doi.org/10.1021/acscpm.9b01074>.
- [6] Novel prominent nylon-1 with excellent dielectric properties and a high Curie point, *J. Mater. Chem. C* 7 (2019) 1641–1650, <https://doi.org/10.1039/c8tc04985h>.
- [7] Preparation and characterization of poly(vinylidene fluoride-trifluoroethylene)/barium titanate polymer nanocomposite for ferroelectric applications, *Polym. Compos.* 38 (2017) 1655–1661, <https://doi.org/10.1002/pc.23734>.
- [8] Synergistic effect of hybrid stainless steel fiber and carbon nanotube on mechanical properties and electromagnetic interference shielding of polypropylene nanocomposites, *Compos. B Eng.* 165 (2019) 662–670, <https://doi.org/10.1016/j.compositesb.2019.02.044>.
- [9] Carbon-based polymer nanocomposites as dielectric energy storage materials, *Nanotechnology* 30 (2018), 062001, <https://doi.org/10.1088/1361-6528/aaf12c>.
- [10] Role of fillers on dispersion of MWNT/fluoroelastomeric composites for high performance dielectric energy storage application, *Journal of Nanoence and Nanotechnology* (2015), <https://doi.org/10.1166/jnn.2015.9529>.
- [11] Superior energy storage performances of polymer nanocomposites via modification of filler/polymer interfaces, *Advanced Materials Interfaces* (2018), <https://doi.org/10.1002/admi.201800096>.
- [12] Dielectric properties and energy storage densities of poly (vinylidene fluoride) nanocomposite with surface hydroxylated cube shaped Ba_{0.6}Sr_{0.4}TiO₃ nanoparticles, *Polymers* 8 (2016) 45, <https://doi.org/10.3390/polym8020045>.
- [13] Enhanced energy storage density in poly (vinylidene fluoride) nanocomposites by a small loading of surface-hydroxylated Ba_{0.6}Sr_{0.4}TiO₃ nanofibers, *ACS Appl. Mater. Interfaces* 6 (2014) 1533–1540, <https://doi.org/10.1021/am4042096>.
- [14] Nanocomposites of ferroelectric polymers with surface-hydroxylated BaTiO₃ nanoparticles for energy storage applications, *J. Mater. Chem.* 22 (2012) 11196–11200, <https://doi.org/10.1039/C2JM30542A>.
- [15] Characterizing the interphase dielectric constant of polymer composite materials: effect of chemical coupling agents, *J. Appl. Phys.* 94 (2003) 4551–4557, <https://doi.org/10.1063/1.1604961>.
- [16] Dielectric investigations and charge transport in PS-PAni composites with ionic and nonionic surfactants, *J. Phys. Chem. Solid.* 133 (2019), <https://doi.org/10.1016/j.jpcs.2019.05.026>.
- [17] Dielectric relaxations in phosphoric acid-doped poly (2,5-benzimidazole) and its composite membranes, *J. Appl. Polym. Sci.* 134 (2017), <https://doi.org/10.1002/app.44867>.
- [18] Effect of protonic acids on the dielectric spectroscopy of polyaniline, *Synth. Met.* 119 (2001) 291–292, [https://doi.org/10.1016/S0379-6779\(00\)01183-8](https://doi.org/10.1016/S0379-6779(00)01183-8).
- [19] Core-shell structured PVDF@BT nanoparticles for dielectric materials: a novel composite to prove the dependence of dielectric properties on ferroelectric shell, *Mater. Des.* 164 (2018), <https://doi.org/10.1016/j.matdes.2018.107556>.
- [20] Core-shell structured poly (vinylidene fluoride)-grafted-BaTiO₃ nanocomposites prepared via reversible addition-fragmentation chain transfer (RAFT) polymerization of VDF for high energy storage capacitors, *Polym. Chem.* 10 (2019) 891–904, <https://doi.org/10.1039/C8PY01706A>.
- [21] Combining RAFT polymerization and thiol-ene click reaction for core-shell structured polymer@ BaTiO₃ nanodielectrics with high dielectric constant, low dielectric loss, and high energy storage capability, *ACS Appl. Mater. Interfaces* 6 (2014) 1812–1822, <https://doi.org/10.1021/am4048267>.
- [22] Poly (vinylidene fluoride)-based nanocomposite employing oriented Bi₂S₃ nanorods with double-shell structure for high dielectric performance and loss suppression, *Compos. Sci. Technol.* 171 (2019) 118–126, <https://doi.org/10.1016/j.compscitech.2018.12.020>.
- [23] Effects of ultralow concentration MXene (nano-Ti₃C₂T_x) on the electric and physical properties of ternary polyvinyl alcohol composites, *Colloids and Surfaces A Physicochemical and Engineering Aspects* 610 (2021) 125929, <https://doi.org/10.1016/j.colsurfa.2020.125929>.
- [24] Enhanced dielectric, electromechanical and hydrophobic behaviors of core-shell AgNWs@ SiO₂/PDMS composites, *Colloid. Surface. Physicochem. Eng. Aspect.* 563 (2019) 59–67, <https://doi.org/10.1016/j.colsurfa.2018.11.067>.
- [25] Improve the dielectric property and breakdown strength of composites by cladding a polymer/BaTiO₃ composite layer around carbon nanotubes, *Polymer* 188 (2020) 122157, <https://doi.org/10.1016/j.polymer.2020.122157>.
- [26] Achieving excellent dielectric performance in polymer composites with ultralow filler loadings via constructing hollow-structured filler frameworks, *Compos. Appl. Sci. Manuf.* 131 (2020) 105814, <https://doi.org/10.1016/j.compositesa.2020.105814>.
- [27] Radio frequency functional capacitors made of all-organic composites of thiourea in field-responsive polymers, *Appl. Phys. Lett.* 92 (2008), 083303, <https://doi.org/10.1063/1.2857498>.
- [28] Piezoelectric energy harvesting based on multiaxial ferroelectrics by precise molecular design, *Matter* 2 (2020) 697–710, <https://doi.org/10.1016/j.matt.2019.12.008>.
- [29] Light-controlled molecular resistive switching ferroelectric heterojunction, *Mater. Today* 34 (2020) 51–57, <https://doi.org/10.1016/j.mattod.2019.09.004>.
- [30] Flexible and transparent high-dielectric-constant polymer films based on molecular ferroelectric-modified poly (vinyl alcohol), *ACS Materials Letters* 2 (2020) 453–460, <https://doi.org/10.1021/acsmaterialslett.0c00086>.
- [31] Record-high thermal stability achieved in a novel single-component all-organic ferroelectric crystal exhibiting polymorphism, *Chem. Commun.* 55 (2019) 9610–9613, <https://doi.org/10.1039/C9CC04434E>.
- [32] Metal-organic complex ferroelectrics, *Chem. Soc. Rev.* 40 (2011) 3577, <https://doi.org/10.1039/c0cs00226g>.
- [33] An order-disorder ferroelectric host-guest inclusion compound, *Angew. Chem. Int. Ed.* 126 (2014) 2146–2150, <https://doi.org/10.1002/anie.201307690>.
- [34] Ultrafast polarization switching in a biaxial molecular ferroelectric thin film: [hdabco]ClO₄, *J. Am. Chem. Soc.* 138 (2016) 15784–15789, <https://doi.org/10.1021/jacs.6b10595>.
- [35] Berezinskii-Kosterlitz-Thouless phase in two-dimensional ferroelectrics, *Phys. Rev. B* 101 (2020) 241402, <https://doi.org/10.1103/PhysRevB.101.241402>.
- [36] Dipole-dipole interaction induced phases in hydrogen-bonded squaric acid crystal, *J. Phys. Condens. Matter* 32 (2020) 285802, <https://doi.org/10.1088/1361-648X/ab7ba1>.
- [37] Polymer bilayers with enhanced dielectric permittivity and low dielectric losses by Maxwell-Wagner-Sillars interfacial polarization: characteristic frequencies and scaling laws, *J. Appl. Polym. Sci.* 136 (2019) 47551, <https://doi.org/10.1002/app.47551>.
- [38] Interfacial polarization in thermoplastic basalt fiber-reinforced composites, *Polymers* 12 (2020) 1486, <https://doi.org/10.3390/polym12071486>.
- [39] Dielectric relaxation and alternating current conductivity of lanthanum, gadolinium, and erbium-polyvinyl alcohol doped films, *J. Appl. Phys.* 112 (2012) 1626, <https://doi.org/10.1063/1.4739752>.
- [40] Dielectric relaxation analysis and AC conductivity of polyvinyl alcohol/polyacrylonitrile film, *Phys. B Condens. Matter* 499 (2016) 24–28, <https://doi.org/10.1016/j.physb.2016.07.002>.
- [41] Influence of Cr₂O₃ nanoparticles on the physical properties of polyvinyl alcohol, *J. Appl. Phys.* 112 (2012), 093525, <https://doi.org/10.1063/1.4764864>.
- [42] High dielectric constant and low dielectric loss poly(vinylidene fluoride) nanocomposites via a small loading of two-dimensional Bi₂Te₃@Al₂O₃ hexagonal nanoplates, *J. Mater. Chem. C* 6 (2018) 271–279, <https://doi.org/10.1039/c7tc04758d>.
- [43] High-energy-density polymer nanocomposites composed of newly structured one-dimensional BaTiO₃@Al₂O₃ nanofibers, *ACS Appl. Mater. Interfaces* 9 (2017) 4024–4033, <https://doi.org/10.1021/acscami.6b13663>.
- [44] Boron nitride filled epoxy with improved thermal conductivity and dielectric breakdown strength, *Compos. Sci. Technol.* 110 (2015) 152–158, <https://doi.org/10.1016/j.compscitech.2015.02.006>.
- [45] Tunable dielectric polarization and breakdown behavior for high energy storage capability in P(VDF-TrFE-CFE)/PVDF polymer blended composite films, *Phys. Chem. Chem. Phys.* 22 (2020), <https://doi.org/10.1039/D0CP01071E>.
- [46] Enhancement of dielectric properties and energy storage performance in 3Y-TZP ceramics with BaTiO₃ additives, *Int. J. Appl. Ceram. Technol.* 17 (2020), <https://doi.org/10.1111/ijac.13403>.